The Ocean Heat Anomaly Budget in ECCOv4: Spatial and Temporal Scale Dependence

Jan-Erik Tesdal* and Ryan P. Abernathey

Lamont-Doherty Earth Observatory, Columbia University, Palisades, New York, USA

**Corresponding author*: Jan-Erik Tesdal, tesdal@ldeo.columbia.edu

ABSTRACT

Variation in upper ocean temperature is a critical factor in understanding global climate variability. Similarly, knowledge of temperature variability in specific ocean regions is crucial to understanding global and regional climate change. The processes controlling regional variations in ocean heat content (forcing, advection and mixing) differ in relevance depending on region and time scale. In the present study, temperature anomaly budgets were described using the ECCOv4 ocean state estimate to describe the balance between atmospheric forcing and ocean transport mechanisms for different basins and oceanic regions and at varying temporal and spatial resolutions. Considering the area-integrated budget for the Atlantic, Pacific and Indian Ocean basins, anomalies in temperature tendency are driven by atmospheric forcing (i.e., sea surface heating). When the contributions of budget terms are spatially resolved, there is a latitudinal pattern where the advection term is most important towards the equator, while forcing becomes increasingly relevant at higher latitudes. However, there are also basin-specific differences affecting which term governs regional budgets. Once sub-basin variation is resolved, the balance between heat budget terms is not particularly sensitive to the scale of spatial aggregation at which the budget is determined. Temporal aggregation shows that atmospheric forcing is more important at short timescales, while at long timescales advection becomes the principal term that determines variability. The linearization of the advective term illustrates that ocean heat variability is due to anomalies in circulation, while anomalies in temperature fields effect focused regions and become more relevant on interannual timescales.

1. Introduction

Earth's oceans play a critical role in regulating the global climate system (Bigg et al. 2003; von Schuckmann et al. 2016). Ocean temperature observations over the last sixty years have shown that the oceans have been warming (Gregory et al. 2004; Levitus et al. 2005; Pierce et al. 2006; Levitus et al. 2012). The majority of the Earth's total energy uptake during recent decades has occurred in the upper ocean (Liang et al. 2015). Global heat uptake in the upper 300 m of the ocean is estimated to have increased during recent decades by $(1.0 \pm 0.1) \times 10^{22}$ J. Oceans respond to climate change by acting as a critical sink of excess atmospheric and land-based heat resulting from greenhouse gases, and therefore tremendous amounts of heat have been absorbed by the ocean, by some estimates more than 90% of excess heat resulting from anthropogenic warming (Barnett et al. 2001, 2005; Pierce et al. 2012; Trenberth et al. 2014). This extra heat results in thermal expansion contributing to global sea level rise (Church et al. 2013).

While, on a global scale, oceans act primarily as a heat sink, heat is also redistributed within and released from the oceans, thereby impacting atmospheric temperatures and the global climate system (Bigg et al. 2003). Ocean heat redistribution determines how effectively oceans can store excess heat due to anthropogenic warming, and played a key role in the 1998-2012 global warming hiatus (Yan et al. 2016; Liu and Xie 2018). In addition, the distribution of excess heat can have important implications for sea ice (Carmack et al. 2015) and marine-terminating glaciers (Holland et al. 2008; Straneo and Heimbach 2013) as well as deep water formation (Robson et al. 2016; Jackson et al. 2016; Menary et al. 2016). Therefore, an understanding of oceanic redistribution mechanisms is important for evaluating the ocean's capacity for attenuating anthropogenic warming by storing excess heat and will enable better predictions in global and regional climate change (Keenlyside et al. 2008; Robson et al. 2012; Roberts et al. 2016).

The heat transfer mechanisms that are responsible for absorption and distribution of heat within the ocean vary in time and space. Variability in heat content for a given region is due to local forcing (represented primarily by solar radiation and heat exchange at the air-sea interface) and transport through advection and mixing (i.e., diffusion). Thus, for any given ocean region, the change in temperature over time is the sum of any change due to forcing (e.g., increased heat flux from the atmosphere), heat flux from advection, and heat flux from diffusion.

Of particular interest has been the relative importance of surface heat flux (SHF) versus ocean dynamics in determining temperature variability in the upper ocean. Atmospheric-driven SHF has a dominant imprint on sea surface temperature (SST) anomalies at diurnal to seasonal timescale (Gill and Niller 1973). Correlations between monthly anomalies of SHF and SST tendency suggest that SST variations over the North Atlantic and Pacific basin are predominantly controlled by atmospheric variations (Cayan 1992). Similarly, a coupled atmosphere-ocean model demonstrated the dominant role of the atmosphere in SST-SHF coupled variability over the extratropics (von Storch 2000). The explanation of the dominant role of the atmosphere in driving ocean variability can be drawn from stochastic climate models (Hasselmann 1976) which assume that stochastic forcing is only relevant in the atmospheric component and, due to its thermal inertia, the oceanic component responds to high-frequency variability (i.e., atmospheric-driven SHF), resulting in low-frequency variability in SST.

By utilizing the stochastic model derived by Hasselmann (1976) and describing the temporal relationship between SST and SHF (i.e., the lead-lag correlation between SHF, SST and its tendency), a series of studies have suggested that for much of the extratropical regions of the global ocean, SST variability is primarily a function of atmospheric-driven SHF (e.g., von Storch 2000; Wu et al. 2006). Bishop et al. (2017) revised the SHF-SST connection using updated observational datasets of SST and SHF that are higher in resolution. They report that SST variability is driven by ocean dynamics in the western boundary currents (WBCs) and the Antarctic Circumpolar Current (ACC). Instead of the lead-lag correlations between SST and SHF, Small et al. (2019) decomposes the latent heat flux (as the major component of SHF) into ocean-driven (i.e., SST) and atmosphere-driven (i.e., wind and humidity) parts. To describe the contribution of each variable to the total variability of latent heat flux, regression coefficients were mapped to reveal SST as the dominant driver in the eastern tropical Pacific and mid-latitude ocean frontal zones such as the WBCs. Wind was found to be dominant in the subtropics and the tropical Indian and Atlantic Ocean while humidity was mostly relevant in the higher latitudes.

Bishop et al. (2017) and Small et al. (2019) described only SST variability. The role of ocean dynamics in heat redistribution is likely to differ when considering a specific depth layer (i.e., depth integrated ocean heat content) versus just the ocean surface. Variability in SST covaries with temperature within the mixed layer (Alexander and Deser 1995), but it remains unclear how SST and the upper ocean (e.g., upper 100, 500 or 700 m) covary, and it is expected that the depth of covariation is not the same between different regions of the ocean.

Roberts et al. (2017) described the global ocean heat budget using observationally-based temperature products and SHF based on atmospheric reanalysis, looking at both the mixed layer and full-depth heat content. Similar to Bishop et al. (2017), they observe heat transport convergence as the dominant term in the mixed layer heat budget for regions of strong ocean currents (e.g., the equator, WBCs and ACC). Besides relatively constrained regions where local air-sea heat fluxes dominate, for extensive regions of the Pacific and Atlantic, ocean dynamics are a relevant component in explaining heat content variability in the mixed layer. For the full-depth budget, ocean heat transport convergence dominates variability with the exception of deep convective sites. Since the analysis was observation based, Roberts et al. (2017) did not explicitly describe ocean transport terms but instead estimated the contribution of transport convergence as a residual.

In addition to observation-based analyses, ocean models can be used to study transport mechanisms explicitly and determine the relative importance of each for a particular region, depth or time. For example, Doney et al. (2007) used an ocean hindcast model to assess the contribution of mechanisms that govern interannual changes in global ocean temperature for the period 1968 to 1997. Regressing each heat budget term on the net annual heat storage anomaly, integrated over the upper 400 m, revealed a dominant role for advective heat convergence in the tropics, while SHF is only relevant in some mid- and high-latitude regions where temperature variability is controlled by both SHF and advective heat convergence. Grist et al. (2010) presented results for the upper 500 m and full-depth temperature variability in the North Atlantic using an eddy-permitting ocean model. Their approach suggested a dominant role for advection in the subpolar and subtropical North Atlantic, while a notable contribution to temperature variability by SHF (i.e., roughly half) is present only in the tropical North Atlantic, which is contradictory to Doney et al. (2007). This apparent discrepancy could be attributed to differences between the climate models used in each study, or how the budgets were resolved (gridded regression in Doney et al. (2007) versus area-integrated budgets in Grist et al. (2010)).

Small et al. (2020) analysed gridded heat budget analysis for both the upper 50 and 400 m in a low- (1°) and high-resolution (0.1°) climate model to describe the contribution by advective convergence versus atmospheric forcing to the total ocean heat content variability. Using the same regression method they confirm findings by Doney et al. (2007) for the upper 400 m with the 1°resolution model. Considering only the upper 50 m, which can be regarded as comparable to the mixed-layer heat content presented in Roberts et al. (2017) and strongly correlated with SST, Small et al. (2020) identifies only the eastern tropical Pacific and Atlantic where ocean heat transport is relevant in the low-resolution model. However, they show that ocean transport is much more relevant in the high-resolution model compared to the low-resolution model. For the upper 50 m, heat content tendency is dominated widely by intrinsic ocean variability and only in the subtropics and higher latitudes of the Pacific is atmospheric forcing relevant. The upper 400 m heat content budget is almost entirely driven by variability in advective heat convergence in the high-resolution simulation.

A series of studies showed that the balance between atmospheric forcing and forcing by ocean dynamics depends on the spatial resolution (Kirtman et al. 2012; Bishop et al. 2017; Small et al. 2019, 2020). By using spatial smoothing, Bishop et al. (2017) show that the importance of ocean-driven variability decreases with increasing spatial scale. This suggests that ocean-driven variability is mainly represented by small-scale features such as eddies. The spatial dependence was further confirmed in climate models for the relationship between SST and SHF (Small et al. 2019) and for the upper ocean heat budget (Small et al. 2020). Similarly, there is a dependence on the temporal scale. While for monthly to seasonal anomalies atmospheric forcing is the dominant term, ocean dynamics becomes more important in establishing interannual and decadal variations in SST and upper ocean heat content (Buckley et al. 2014, 2015). The time scale at which a switch occurs from atmospheric- to oceanic-driven scenario is regionally dependent (Buckley et al. 2015). By using a low-pass filter Bishop et al. (2017) show that importance of ocean-driven variability increases with increasing time scale. Small et al. (2019) expands the time-dependency to sub-monthly variability and show that the ocean-driven signal becomes relevant in the WBCs for time scales longer than 5 days.

Most observation-based analyses of temperature variability have been focused on the sea surface for which satellite data provides sufficient spatial and temporal resolution. Representing temperature variability below the surface is challenged by spatial and temporal bias due to incomplete coverage by historical observations. Ocean and climate models have been applied to run hindcast simulations in order to have a complete representation of ocean temperature variability and of the underlying mechanisms driving this variability. However, these hindcast simulations are usually unconstrained and key variables of the model output (e.g., SST, SSH) are only compared with available observations post-simulation to assess fidelity. An ocean model that assimilates ocean observations as part of the simulation can be considered the âĂIJbest of both worldsâĂİ by bringing historical observations and a physically consistent representation of ocean processes together to describe temperature variability within the ocean.

In this paper, we conduct an investigation of the drivers of variability in ocean heat content using the Estimating the Circulation and Climate of the Ocean consortium (ECCO) state estimate. The third release of version 4 (ECCOv4) provides a physically consistent ocean state estimate covering the period 1992-2015. Its solution is the output of the Massachusetts Institute of Technology general circulation model (MITgcm) assimilated to available observations for the period 1992 to 2015, which has been thoroughly assessed and found to be a coherent and accurate representation of the ocean state (Forget et al. 2015). In addition to providing closed tracer budgets, ECCOv4 offers detailed diagnostic information about the simulation, making it possible to identify the contributions of specific mechanisms to those budgets. Because of the model's conservation rules, there are no unidentified sources of heat, which makes ECCOv4 well suited as a reanalysis in order to investigate heat content variability in the ocean over recent decades.

The ECCO state estimate has been employed in a number of studies to evaluate ocean heat content variability and the mechanisms that drive it. It has been used to study meridional heat transport and heat storage rates in the Atlantic (Piecuch and Ponte 2012), highlighting the importance of advective processes. Furthermore, it has been used to describe the Ekman and geostrophic components of advective convergence in the North Atlantic mixed layer (Buckley et al. 2014) and describe variability in total advective heat, Ekman and geostrophic convergence due to anomalies in velocity and temperature and the covariability of these anomalies (Buckley et al. 2015). A recent study by Piecuch et al. (2017) also decomposed the advective heat convergence in ECCOv4 temporally and showed that decadal heat content variability in the subpolar North Atlantic is mostly due to velocity anomalies acting on the mean temperature. Buckley et al. (2014) noted a combination of geostrophic, diffusion and bolus transport convergence for the eastern half of the North Atlantic subpolar gyre in explaining the total heat tendency at interannual and decadal time scales.

These particular ECCO studies determined regional rather than global ocean heat budgets. This prompted our present work to expand on the recent study of Small et al. (2020) by including higher latitudes and using an ocean state estimate that assimilates ocean observations. This study will present regional heat budgets but also focus on the global distribution of regression coefficients for key drivers of ocean temperature variation, comparable to Doney et al. (2007) or Small et al. (2020). We represent budgets by region to facilitate comparison between basins and oceanic regions, anticipating that the mechanisms driving the heat budget are not just a function of latitude but are also unique to specific basins. Previous findings allude to the different spatial patterns between each basin. For example, Small et al. (2019) showed that the latent heat flux is driven by variations in SST in the equatorial Pacific, while in the equatorial Atlantic latent heat flux is driven mainly by wind. Also, it is expected that mechanisms associated with climate modes such as the El Nino Southern Oscillation are operating in one basin (e.g., Pacific) and do not have the same response in other basins (e.g., Atlantic). Thus, the mechanisms that control heat variability at the ocean surface and the upper ocean layer need to be distinguished by a detailed heat budget analysis. This study provides further investigation of how spatially integrated budgets differ among the basins.

In the following Section 2, we derive a budget equation describing the temperature tendency anomaly as the sum of distinct variations in ocean heat processes simulated by the MITgcm model. We further introduce a method to quantify the contribution of each budget term to the total variability of temperature. This method has much in common with the approach introduced in previous work for studying sea-surface temperature variability (Small et al. 2019) and upper ocean heat budgets (Doney et al. 2007; Small et al. 2020). In this study, we consider a range of ocean depths and spatial domains for area-integrated budgets, as well as evaluating the contribution of each budget term at a range of spatial and temporal resolutions.

In Section 3, we present the results of our budget analysis with the focus on evaluating the relative importance of each budget term in controlling changes in ocean heat content. In the first component of the study we consider the balance of terms in the ocean heat budget at the basin, subsection and regional scale. In its most basic form, the budget analysis addresses the balance between forcing, advection, and diffusion. It shows that the forcing term is the main driver of ocean heat content at short timescales, whereas at long timescales advection becomes the principal term that determines heat content. We further show that the advection term is the most important driver of heat content in the tropics, while at higher latitudes forcing is increasingly relevant. We also perform a linearization of the advection terms and show that anomalous advection of the mean temperature field is the main driver of temperature variability for the ocean in general. We then examine how the budget varies at different spatial aggregations scales. The analysis reveals that the balance of terms observed in the original 1°grid does not notably shift with spatial aggregation. These results are further discussed in Section 4, with concluding remarks and suggestions for future observational work.

2. Methods

a. Anomaly heat budget in ECCOv4

We use version 4 of ECCO (Forget et al. 2015) to describe heat variability in the global ocean. The ocean heat variability is described with the anomaly budget of temperature that is derived from release 3 of ECCOv4. The budget equation for temperature can be expressed in the general form as

$$\frac{\partial \theta}{\partial t} + \nabla \cdot (\theta \mathbf{u}) = -\nabla \cdot \mathbf{F}_{\text{diff}} + F_{\text{forc}} \tag{1}$$

The temperature budget is expressed as change in temperature over time ($\frac{\partial \theta}{\partial t}$) as a function of the convergence of heat advection ($-\nabla \cdot (\theta \mathbf{u})$) and heat diffusion ($-\nabla \cdot \mathbf{F}_{\text{diff}}$) plus downward heat flux from the atmosphere (F_{forc}). In order to derive the anomaly budget of temperature, we first determine the budget equation of the monthly climatological mean temperature, which can be done by recognizing that each variable can be expressed as the monthly mean plus its anomaly (i.e., climatology + seasonal anomaly). We derive the monthly mean budget by applying Reynolds averaging to Equation 1, and replacing each term by its monthly mean plus anomaly. The monthly mean and anomaly of variable X is denoted as $\overline{X}^m$ and X', respectively. The monthly anomaly budget is then derived by subtracting the monthly mean equation from Equation 1, which removes the mean seasonal cycle and returns the month-to-month interannual variability. The central equation for our budget analysis is thus

$$\frac{\partial \theta'}{\partial t} = F_{\text{forc}}{}' - \nabla_h \cdot (\mathbf{u}' \overline{\theta}^m) - \frac{\partial}{\partial z}(w' \overline{\theta}^m) - \nabla_h \cdot (\overline{\mathbf{u}}^m \theta') - \frac{\partial}{\partial z}(\overline{w}^m \theta') - \nabla \cdot (\mathbf{u}'\theta' - \overline{\mathbf{u}'\theta'}^m) - \nabla \cdot \mathbf{F}_{\text{diff}}{}' + R \tag{2}$$

The first term on the right-hand side of Equation 2 ($F^{\theta}_{\text{forc}}{}'$) is the anomalous forcing (i.e., anomalous air-sea heat flux). The convergence of the heat advection anomaly is described by a sum of terms resulting from the temporal decomposition of the advective fluxes. The advective heat flux is decomposed to a linear term due to temporal anomalies of the velocities, a linear term due to anomalies in temperatures, and a nonlinear term due to the covariance between the two anomalies. Furthermore, the two linear terms are separated into horizontal and vertical components. Technically, advective heat transport should only be calculated for flows with zero net mass transport (Warren 1999). However, we find it informative to separate horizontal and vertical components, recognizing that only the sum of the horizontal and vertical components has zero net mass transport. (Readers who dislike this choice can simply sum together the two components.) The first two advective terms are the horizontal ($-\nabla_h \cdot (\mathbf{u}'\overline{\theta}^m)$) and vertical ($-\frac{\partial}{\partial z}(w'\overline{\theta}^m)$) heat flux caused by velocity anomalies acting on the mean temperatures. The following two terms are the horizontal ($-\nabla_h \cdot (\overline{\mathbf{u}}^m\theta')$) and vertical ($-\frac{\partial}{\partial z}(\overline{w}^m\theta')$) heat flux due to mean velocities acting on temperature anomalies. The nonlinear advective term ($-\nabla \cdot (\mathbf{u}'\theta' - \overline{\mathbf{u}'\theta'}^m)$) describes the difference in advection given by the correlation between the velocity and temperature anomalies and its climatological mean. Finally, Equation 2 includes the anomalous convergence of diffusion ($-\nabla \cdot \mathbf{F}^{\theta}_{\text{diff}}{}'$) and a residual term ($R$).

It should be noted that the derivation of this anomaly heat budget necessitates a residual term to yield an exact balance. The velocity terms in Equation 2 are the residual mean velocities containing both the resolved (Eulerian) and parameterized eddy induced transport. Because the advective temperature flux is derived with monthly-averaged model output of mass weighted velocities and temperature, the budget terms miss the effect of submonthly covariation. Furthermore, the derivation neglects temporal decomposition of the scaling factor corresponding to the non-linear free surface in ECCOv4 (Adcroft and Campin 2004; Campin et al. 2004). The residual term in Equation 2 addresses these points by accounting for any variability that is ignored in the offline estimation of the advective fluxes. As we shall see, the residual is small nearly everywhere.

b. Regression Analysis

The ECCOv4 outputs permit us to calculate the anomaly budget timeseries at each point in the global 3D grid. This is too much information to comprehend or visualize. To understand which terms drive heat content variability, we consider the correlation between the left-hand side of (2)–the actual tendency, denoted y–and the terms on the right-hand side, denoted x.

We define the covariance ratio for a particular term x as

$$r_x = \frac{\sigma(x,y)}{\sigma(y)^2} \tag{3}$$

where $\sigma(x,y)$ is the covariance between x and y and $\sigma(y)^2$ is the variance of y. In any particular heat budget, the covariance ratio describes the contribution of each budget term to the total temperature tendency. Since the total tendency is the sum of all the budget terms, the sum of the covariance ratios must equal one. A positive covariance ratio implies a positive contribution (and correlation) to the total tendency, and a negative value implies a negative contribution (and an inverse correlation) to the total tendency. For the anomaly heat budget (Equation 2), $\overline{y'}$ and $\overline{x'}$ equal to zero, such that the covariance ratio can be expressed as

$$\frac{\sigma(x,y)}{\sigma(y)^2} = \frac{\int_{t_0}^{t_1} x(t)y(t)dt}{\int_{t_0}^{t_1} y(t)y(t)dt} \tag{4}$$

This formula, discretized into monthly values, is how we analyze the data.

c. Basin-scale analysis

Three major basins (Pacific, Atlantic, Indian) are considered and further subdivided into northern (in the case of Pacific and Atlantic), tropical and southern sections (Figure 1). In addition, the Southern Ocean (SO) and the subpolar North Atlantic (SPNA) are included as distinct regions overlapping the more categorical regions because of their important role in ocean heat storage and global climate (Keenlyside et al. 2008), and to allow comparisons with previous studies (e.g., Piecuch et al. 2017). Ocean regions considered in this study are listed in Table 1. The budget terms were summed over each ocean region, such that the heat budget is assessed separately for each region. The contribution of each budget term is determined by comparing the covariance ratios. Since the total tendency of heat variability is equal to the sum of the individual heat budget terms, and the sum of the covariance ratios for each term should equal 1.0, the covariance ratio for a given term can be regarded as the contribution of that term to the variability of the heat content for a given ocean region and time scale.

d. Spatial and temporal aggregation

All of our analysis uses the ECCOv4 native lat-lon-cap (llc) grid which is organized in 13 tiles, each including 90 by 90 grid cells (Forget et al. 2015). The spatial resolution of the llc grid varies globally but is on average 1°×1°. In order to retain closed budgets at each spatial scale, we do not spatially interpolate the llc grid to a regular latitude-longitude grid, but instead spatially aggregate grid points only within each tile. This is done by binning the grid points into equal windows of size n-by-n and summing their values. To ensure conservation of properties, the aggregation is done by summing n-by-n bins where n can only be a number that ensures an exact factor of 90. Therefore, n-by-n binning included values of n equal to 2, 3, 5, 6, 9, 10, 15, 18, 30 and 45. Given that the spatial resolution of the original dataset (i.e, $n = 1$) is about 1°×1°, the degree resolution is approximately $n°\times n°$ for a given value of n. The highest n value ($n = 45$) corresponds to approximately 45°×45°, which can be considered a basin-wide scale and would be comparable to the categorical regions as shown in Figure 1.

The ECCOv4 output is provided as monthly-averaged fields from January 1992 to December 2015. The temperature tendency anomaly (left-hand side of Equation 2) is derived from monthly snapshots at the beginning and end of each month. Temporal aggregation was done on the monthly time series of the budget terms by averaging over set intervals (3-month, 6-month, 1-year, 2-year, 3-year, 4-year, 5-year and 10-year).

3. Results

Ocean heat content variability was investigated in this study, in particular as it is affected by forcing, advection and diffusion, and how differing spatial and temporal scales impacts the balance of these terms in the overall heat budget. The terms were derived by the anomaly heat budget as presented in Equation 2. We first present results of a regional analysis at fixed spatial scale for the general mechanisms (forcing, advection and diffusion) and assess the extent of a residual term (i.e., variation in the budget that is not attributable to any mechanism). We then present the dependency of each term on the temporal scale of the analysis and the depth of integration, followed by analysis that decomposes the advection convergence into components reflecting velocity variability, temperature variability and their covariability. Lastly, we present global distributions of the covariance ratio for the different terms in the anomaly heat budget and test its sensitivity to increasing spatial aggregation.

a. Regional and basin-wide heat budgets

At the basin scale of the upper ocean (most commonly defined as < 700 m; Piecuch et al. (2017); Robson et al. (2016)), forcing is the major contributing term in determining the total tendency for relatively short (e.g., monthly) time scales. This is clearly shown by the covariance ratios of the monthly budget terms integrated over the upper 700 m (Table 2). All the major basins (i.e., Pacific, Atlantic and Indian Ocean) have a high covariance ratio for forcing. The covariance ratios for forcing are highest in the Atlantic, ranging from 0.46 in the South Atlantic to 0.85 in the North Atlantic (i.e., forcing is responsible for 85% of total heat variability in the North Atlantic). As a secondary term of the heat budget, advection is the only other term that contributes to the total tendency. The covariance ratios for advection range from 0.15 in the North Atlantic to 0.64 in the tropical Indian Ocean. By contrast, the covariance ratios for diffusion across all different ocean regions is near zero; therefore, at this spatial and temporal scale, diffusion is negligible for the total variability of temperature. Results in Table 2 also indicate that the residual term has no influence on the variability of the temperature tendency, at least in the case of basin-wide scales and monthly frequency.

Whereas forcing dominates the ocean heat budget at the basin scale, the balance of contributing mechanisms shifts to some extent when moving to subdivisions of the different basins. Forcing accounts for 80% of the total temperature variability of the entire Pacific Ocean, but subdividing the Pacific into northern, tropical and southern sections reduces that contribution to 37%, 43% and 47%, respectively. For the Atlantic Ocean, the tropical subdivision shows a covariance ratio for advection that is moderately higher than that for forcing (0.54 and 0.46, respectively), while forcing remains dominant (0.73 to 0.85) in the high latitudes. A similar situation is observed in the Indian Ocean, where the contribution of advection reaches 64% in the tropical subsection. Advection is the major contributor to heat variability in the North Pacific (63%), but has lower contribution in the North Atlantic and subpolar North Atlantic regions (15% and 29%, respectively). These data show that in general, tropical regions are associated with greater contributions to the heat budget by advection, while regions at higher latitudes tend to have greater contributions by forcing (with the exception of the North Pacific). This illustrates that even at the ocean basin scale, advection can be an important contributor to monthly heat variability, although forcing remains the dominant driver in the major basins (i.e., Atlantic, Pacific, Indian).

1) Dependence on time scale

In the upper ocean (< 700 m) at the basin scale, forcing is the major term in determining total tendency at relatively short (e.g., monthly) time scales (Table 2). The question is whether the balance of terms could be different at longer temporal scales (e.g., annual, pentad or decadal). The budget terms for the basins and subsections were first evaluated at monthly resolution, and then temporally aggregated over 3-month, 6-month, annual, 2-year, 3-year, 4-year, 5-year and decadal intervals. The aim of these multiple temporal aggregations was to clearly illustrate the shifts in the balance of budget terms and whether these occur gradually or appear at a particular timescale.

The time series of the temperature budget change depending on the temporal aggregation scale, as illustrated by the budget terms for the upper 700 m of the subpolar North Atlantic (Figure 2). In this example, forcing and advection are the only dominant drivers of the variability in temperature, and forcing has the highest relative importance at the temporal aggregation interval of one month. However, as the temporal aggregation intervals increase from one month to five years, the relative importance of forcing decreases as the relative importance of advection increases, such that advection becomes the dominant term at the five year aggregation interval. At this interval, the total tendency shows a decreasing trend driven by advection, whereas the forcing term is always positive. It is apparent, then, that the dominant terms in the heat budget change depending on the time scale over which the heat budget is determined. The anomalous change in temperature due to diffusion in the subpolar North Atlantic is generally small (Figure 2), but more importantly the variation in total tendency has little correlation with diffusion-related changes. The temperature variability associated with the residual term is effectively zero across all temporal aggregations.

2) Dependence on depth of integration

As the balance of dominant mechanisms in the heat budget varies with ocean region, there is also the question of how the balance in the regional budgets can differ with the depth of integration. For the major oceanic basins and subsections (Figure 1; Table 1), the horizontal scale was fixed while the vertical scale was varied by depth of integration (50 m, 100 m, 300 m, 700 m, 2000 m, and 6000 m/full-depth). The contribution of each term to the heat budget (i.e., the covariance ratio) for a given ocean region was calculated for each temporal scale and depth of integration in order to describe how the relative importance of different mechanisms change as the vertical integration and temporal scale are varied. Over the range of temporal and vertical integration scales studied, the principal driving mechanisms were consistently forcing and advection, and the balance between these mechanisms changed substantially according to the specific time or depth scale (Figure 3).

The overall pattern revealed in Figure 3 is a shift with increasing time aggregation scale from forcing to advection as the dominant factor in the heat budget, although in most cases this shift is apparent only at depths of 300 m or greater. As would be expected, forcing is the dominant term at shallower depths of integration in almost all regions. As integration is done over deeper depth levels, it is exclusively advection that becomes increasingly dominant, whereas contributions of forcing and diffusion decline. In some ocean regions, notably the North and South Pacific and the North Atlantic including the SPNA, covariance ratios for forcing are very close to 1.0 for the upper 50 and 100 m across all temporal scales. These regions also show a sharp shift between the upper 100 m and 300 m, where forcing become less important and in turn advection becomes the greater influence.

The tropical ocean regions do not feature this strong influence by forcing in the upper 50-100 m. The tropical Pacific in particular displays a relatively weak influence of forcing at these depths, where at temporal scales greater than 3 years, the shift along depth actually reverses, with higher covariance ratios for advection in the upper 50 to 100 m and the contribution by forcing becoming prominent only when integrating over deeper depths. Also to some extent in the Southern Ocean there is a lack of the shifting balance between forcing and advection seen in other regions. Here, the covariance ratios for advection are fairly insensitive to the depth of integration (at least for temporal means less than 3 years). An exception to the pattern of shifting covariance ratios along the temporal aggregation scale is the North Pacific, where no decline is observed in the covariance ratios for forcing, across all depth levels and for most of the temporal aggregations. The contribution by advection at greater depths are also relatively unchanged, except for pentad and decadal time scales.

The diffusion term exhibits only minor influence on the heat budget, and this occurs only in some regions and at longer time scales. One exception is the SPNA, where diffusion appears to compensate the strong influence by forcing at shorter time scales and by advection at longer time scales. However, diffusion only has an effect in the upper 50 and 100 m. Finally, the residual term (i.e., any variation in temperature that cannot be attributed to a particular mechanism), is close to zero in almost all cases, thus confirming the physical consistency of ECCOv4 in closing the ocean heat budget through forcing, advection and diffusion.

As noted previously, the sum of the covariance ratios for each term is equal to 1.0. There are cases where the covariance ratio of a given term is greater than 1.0 or less than -1.0. These cases occur with large temporal aggregation intervals (>1 year), as well as some instances in the upper 50-100 m. Covariance ratios that are below -1.0 or above 1.0 are due to covariances greater than the variance of the total tendency, which indicates a compensation or dampening of one term against other terms. For example, in the case of the SPNA, forcing and advection is proportional to and thus contribute to temperature tendency (indicated by positive covariance ratios), while the negative covariance ratio of diffusion indicates an inverse relationship with the total tendency, such that diffusion counteracts advection and forcing.

3) Temporal decomposition of the advective heat convergence

It is possible to refine the description of advection in the heat budget equation as the sum of linear and nonlinear components (Equation 2). This temporal decomposition of the advection term quantifies the degree to which the anomaly in advection is caused by anomalies in circulation, temperature, or covariation of anomalies in both (referred here as the nonlinear advection term). The covariance ratios in Figure 4 indicate that the variation in advection is primarily driven by the anomalous variation in advection of mean temperature ($-\nabla\cdot(\mathbf{u}'\overline{\theta}^{m})$). There are some exceptions, at decadal time scales (i.e., 10A) in South Indian Ocean or Southern Ocean, and at time scales greater than three years in the North and South Atlantic, where covariance ratios close to 1.0 are observed for mean advection of anomalous temperature ($-\nabla\cdot(\overline{\mathbf{u}}^{m}\theta')$) and therefore are more dominant compared to $-\nabla\cdot(\mathbf{u}'\overline{\theta}^{m})$. Substantial positive or negative values of the covariance ratio also suggest discernible contribution of $-\nabla\cdot(\overline{\mathbf{u}}^{m}\theta')$ in the North and South Pacific, mostly at the surface and for longer temporal scales ($\geq$ 4 years). The covariance ratio of the nonlinear advective term ($\nabla\cdot(\mathbf{u}'\theta' - \overline{\mathbf{u}'\theta'}^{m})$) is effectively zero at the basin-scale across all regions.

Comparison of the horizontal and vertical components of the linear terms of advection reveals that the anomalous horizontal advection of mean temperature ($-\nabla_h\cdot(\mathbf{u}'\overline{\theta}^{m})$) is dominant for essentially every ocean region (Figure 5). The vertical component of the anomalous advection of mean temperature ($-\frac{\partial}{\partial z}(w'\overline{\theta}^{m})$) dampens the effect of the horizontal component and generally contributes to a reduction in the total variability. As $-\nabla_h\cdot(\mathbf{u}'\overline{\theta}^{m})$ contributes to a positive or negative temperature anomaly, $-\frac{\partial}{\partial z}(w'\overline{\theta}^{m})$ counteracts this effect. This partial compensation is evident for example in the SPNA, where $-\nabla_h\cdot(\mathbf{u}'\overline{\theta}^{m})$ and $-\frac{\partial}{\partial z}(w'\overline{\theta}^{m})$ are almost always of opposite sign (Figure 2, f-j). Despite the compensation, it is $-\nabla_h \cdot (\mathbf{u}'\overline{\theta}^m)$ that determines the sign of the total advective convergence ($-\nabla \cdot (\mathbf{u}\theta)$), because the mostly positive covariance ratios for advection are reflected by $-\nabla_h \cdot (\mathbf{u}'\overline{\theta}^m)$, and the compensation by $-\frac{\partial}{\partial z}(w'\overline{\theta}^m)$ is only a fraction of $-\nabla_h \cdot (\mathbf{u}'\overline{\theta}^m)$. Obviously, at deeper depths of integration, the dampening effect of $-\frac{\partial}{\partial z}(w'\overline{\theta}^m)$ decreases.

In some cases, notably the South Atlantic and South Indian Oceans, the mean horizontal advection of anomalous temperature ($-\nabla_h \cdot (\overline{\mathbf{u}}^m\theta')$) contributes to the total temperature variability when looking at temporal aggregations of 2-year means or greater (Figure 5). In these cases, there is no associated dampening effect observed in the corresponding vertical component. It is interesting to note that $-\nabla_h \cdot (\mathbf{u}'\overline{\theta}^m)$ is also often counteracted by $-\nabla_h \cdot (\overline{\mathbf{u}}^m\theta')$. However, with the exception of the South Atlantic and South Indian Oceans, this effect appears to be very minor as shown by covariance ratios for $-\nabla_h \cdot (\overline{\mathbf{u}}^m\theta')$ that are close to zero. Again, Figure 2 f-j illustrates this partial compensation for the SPNA where the respective terms are of opposite signs.

b. Global distribution of relevance for key budget terms and its dependency on spatial scale

The heat budget analysis to this point demonstrates the relative contributions of budget terms at the basin scale (as defined in Figure 1 and Table 1), corresponding to a high level of spatial aggregation. For the highest level of aggregation (i.e., summing the budget terms over the global scale), the contribution of advection and diffusion to the heat budget is zero. Thus, as the aggregation scale increases, the balance of terms should shift such that the forcing term increases in relative importance (with advection and diffusion increasingly less important). In the upper ocean (< 700 m) at the major basin scale (e.g., summing over the entire Atlantic), forcing is the dominant heat budget term (Table 2). It is also of great interest to determine how the balance of relative contributions by the different budget terms changes when moving from the original spatial resolution of approximately $1°\times1°$ to coarser resolutions.

When summing over the basin scale, the balance in the ocean heat budget is dominated by $F_{\text{forc}}{}'$ and $-\nabla\cdot(\mathbf{u}'\overline{\theta}^{m})$. These terms also show the most pronounced signal at the original 1°×1° resolution (Figure 6). For the upper 700 m, there are distinct global patterns of covariance ratios of the budget terms that are largely meridional. The covariance ratios for $F_{\text{forc}}{}'$ are essentially zero in the tropics and gradually increase towards higher latitudes (Figure 6a). In contrast, $-\nabla_h\cdot(\mathbf{u}'\overline{\theta}^{m})$ reveals a broad pattern of high covariance ratios in the tropics and subtropics and much lower covariance ratios at polar and subpolar latitudes (Figure 6b). The nearly opposite pattern is observed for $-\frac{\partial}{\partial z}(w'\overline{\theta}^{m})$ with weakly negative covariance ratios at most latitudes, except the Arctic and Southern Ocean where covariance ratios are zero or slightly positive (Figure 6d).

Accounting for the compensation effect of the vertical component (i.e., adding the correlations in Figure 6 b and d), the sole driver of the heat budget at the ECCOv4 grid scale in lower latitudes (30°S to 30°N) is the anomalous circulation acting on the mean temperature field. The mean horizontal advection of temperature anomalies ($-\frac{\partial}{\partial z}(\overline{w}^{m}\theta')$) is only relevant at higher latitudes and in discrete locations, such as in boundary and circumpolar currents (Figure 6c). It should be noted that covariance ratios of other terms in the heat budget (e.g., diffusion) do show some spatial patterns, but are generally close to zero.

Zonal mean plots of the covariance ratios (Figure 7) confirm $-\nabla\cdot(\mathbf{u}'\overline{\theta}^{m})$ as the dominant term in the temperature budget in the lower latitudes. For different integration depths (i.e., 100 m, 300 m, 700 m) the influence of this term increases at higher latitudes where the zonal mean covariance ratios are highest between 10°S to 10°N at an integration depth of 100 m, between 20°S to 20°N at an integration depth of 300 m, and between 30°S to 30°N at an integration depth of 700 m. This pattern is mirrored by the vertical component of anomalous advection, and so represents a dampening effect on the horizontal component. The zonal means also confirm that $F_{\text{forc}}{}'$ increasingly contributes more to the heat budget towards higher latitudes.

In the upper 100 m, the covariance ratios of both horizontal and vertical component of the anomalous advection ($-\nabla \cdot (\mathbf{u}'\overline{\theta}^m)$) are large but of opposite sign. Thus, when accounting for the compensation, these components have only minor influence across most of latitude bands and are only dominant around the equator between 10°S to 10°N. As the horizontal and vertical advection compensate each other, $F_{\mathrm{forc}}{}'$ is the dominant term in the heat budget of the upper 100 m.

For annual and pentad averages, $-\nabla_h \cdot (\overline{\mathbf{u}}^m\theta')$ also becomes more important, especially in the southern high latitudes (corresponding to the Southern Ocean). For monthly and annual time averages $-\frac{\partial}{\partial z}(w'\overline{\theta}^m)$ is the only term that counteract total variability. There is only minor compensation by diffusion ($-\nabla \cdot \mathbf{F}_{\mathrm{diff}}{}'$) seen for the upper 100 m.

For pentad averages there are multiple terms whose zonal mean of covariance ratios are negative. This indicates that in some latitudes there can be strong anticorrelation at pentad time scale for terms that usually contribute to the total tendency (i.e., have positive covariance ratios). At latitude 70°N, the nonlinear advective term ($-\nabla \cdot (\mathbf{u}'\theta' - \overline{\mathbf{u}'\theta'}^m)$) shows a strong compensation which is not apparent at higher frequencies (monthly and annual). At 60°S we see that $-\nabla_h \cdot (\mathbf{u}'\overline{\theta}^m)$, which is generally contributing to total tendency, dampens variability by counteracting $-\nabla_h \cdot (\overline{\mathbf{u}}^m\theta')$ and $F_{\mathrm{forc}}{}'$.

The balance of contributing terms in the heat budget equation varies according the spatial and temporal scales on which the terms are derived. The remaining question is how the importance of each term (i.e., forcing, advection, diffusion) changes as spatial aggregation changes from the original 1°×1° grid to increasingly coarse aggregation scales (e.g., 2°×2°, 10°×10°, 45°×45°).

Table 3 lists the global average of covariance ratios of each budget term listed for each spatial aggregation scale, starting with the original resolution (1 × 1) to a maximum binning level of 45 × 45. In general, global mean covariance ratios for the upper ocean are remarkably insensitive to spatial scale, changing only gradually when spatially aggregating the fields (Table 3). There is only a gradual increase in forcing with larger aggregation scales. By the same token, contribution by advection only gradually decreases. The global mean covariance ratios for diffusion, the mean vertical advection of mean temperature, as well as the nonlinear advection term remain effectively zero across all spatial scales.

Forcing and anomalous advection ($F_{\mathrm{forc}}{}'$ and $-\nabla \cdot (\mathbf{u}' \overline{\theta}^{m})$) are similarly sensitive across all latitudes with only a few exceptions (Figure 8). The zonal means of covariance ratios for forcing shift slightly more in the high latitudes (especially in the Northern Hemisphere). The strongest shifts in the covariance ratios for anomalous advection are in the mid-latitudes, especially in the Southern Hemisphere. Advection remains the main contributor in the low latitudes even at the largest aggregation scales (45 × 45).

The relatively low sensitivity of the terms to spatial aggregation remains true when looking at different temporal scales (i.e., monthly, annual or pentad averages) as well for different depths of integration (i.e., upper 100 m, 300 m, 700 m). There are only a few cases where spatial aggregation cause a shift in the balance of terms. For example, pentad averages of forcing at 70°N result in high covariance ratios (>1.0) only at smaller spatial scales. This is seen across the upper 100 to 700 m. On the other hand, $-\nabla \cdot (\mathbf{u}' \overline{\theta}^{m})$ is affected by spatial aggregation as covariance ratios shift from positive to negative values in the upper 100 m (Figure 8).

Regional heat budgets (Figures 3-5) suggest that the contribution of advection (in particular $-\nabla \cdot (\mathbf{u}' \overline{\theta}^{m})$) increases as the temporal scale increases. The same can be observed at the grid scale (Figures 7 and 8). The latitude band where the zonal mean covariance ratio of $-\nabla \cdot (\mathbf{u}' \overline{\theta}^{m})$ is greater than $F_{\mathrm{forc}}{}'$ expands slightly, primarily in the Northern Hemisphere, as temporal scale increases from monthly to pentad averages. This has important implications for the interpretation of decadal signals in ocean heat content. As this study suggests, the anomalous advection of mean temperature plays a major role in decadal trends of heat content at grid scale as well as for basin-wide regions.

4. Conclusion

This study investigated the contribution of individual mechanisms to ocean heat content variability at a range of spatial and temporal scales. The balance in the ocean heat budget is mainly between surface forcing and convergence in anomalous advection of the mean temperature field ($-\nabla \cdot (\mathbf{u}'\overline{\theta}^m)$). Forcing is dominant only at the major basin scale. At smaller spatial scales, anomalous advection becomes the prominent term in the heat budget. Anomalous advection is by far the dominant driver of ocean heat change in the tropics, while forcing contributes to local heat variability only at higher latitudes. There are also differences in the heat budgets among basins. For example, the difference between the North Pacific and Atlantic illustrate difference balances between the budget terms despite being at the same latitudes. The AMOC may explain this difference, as there is no deep convection in the northern latitudes of the North Pacific corresponding to the AMOC, which plays a key role in the North Atlantic heat budget. There are regional features (e.g., boundary currents, circumpolar currents) where the mean (horizontal) advection of anomalies is relevant to total heat variability.

With increasing depths of integration, the balance between forcing and advection shifts towards higher contribution of the advective terms. It is evident that contribution of forcing is generally greater at shallower layers (i.e., upper 50-100 m) as it is represented mostly by solar radiation and heat exchange at the air-sea interface. As the depth of integration increases, advection becomes more important and forcing diminishes in the lower latitudes. When integrating over the entire water column, forcing remains relevant only in the higher latitudes.

As opposed to recent studies by Bishop et al. (2017) and Small et al. (2019, 2020), we find that spatial aggregation of the gridded ECCOv4 fields to coarser resolutions does not substantially change the balance between forcing and advection. The overall patterns remain the same up to a factor of 45, which approaches basin-wide integration. This low sensitivity of the heat budget to aggregation scale is surprising, as the expectation would be that the balance of mechanisms in the budget shifts substantially towards forcing as aggregation occurs over larger scales. However, only a gradual increase in the contribution of forcing was observed as the spatial scale coarsened, such that forcing is dominant only at the major basin to global scale. Similarly, the contribution by advection decreases only gradually with coarsening, mostly in the high latitudes. Advection remains the main contributor in the low latitudes, even at the largest aggregation scale (i.e., 45 × 45). The key to explaining the difference to previous studies (Bishop et al. 2017; Small et al. 2019, 2020) is that the spatial resolution of the ECCOv4 state estimate is already too coarse to resolve mesoscale dynamics. The only possible exception is the tropical oceans, where the the ocean-driven signal occurs on such a large scale that it is resolved in ECCOv4.

The heat budget appears to be more sensitive to the temporal scale. Averaging over longer time intervals (i.e., varying the temporal mean from monthly to decadal), results in a decrease in forcing as the major contributor, concomitant with an increase in the contribution by advection. This transition, from forcing to advection as the dominant driver of heat variability as temporal aggregation increases, is common in most basin-wide regions and at all grid scales. This suggests that forcing generally acts on shorter time scales, while advection is increasingly important at longer time scales. Interestingly, it is mostly the mean advection of anomalies that becomes dominant at longer time scales. The greater importance of mean advection of anomalous heat content at long time scales is consistent with studies which treat the long-term ocean-heat-uptake problem as a passive tracer transport phenomenon (Zanna et al. 2019).

The spatial pattern of covariance ratios we have described in this study is also broadly compatible with the conclusion from Armour et al. (2016), who studied the effect of mean circulation on temperature trends in the Southern Ocean. They conclude that south of the Antarctic Circumpolar

Current (ACC), mean circulation is responsible for the relatively weak SST trends. We also find that mean circulation of anomalous temperatures is the dominant driver of temperature variability in the Southern Ocean at longer time scales. (Figures 6 and 7) and that atmospheric forcing plays a lesser role here. This is in contrast to the high latitudes of the Northern Hemisphere, where we find forcing to be more dominant. While our focus was not on temperature trends, we have shown that the Southern Ocean is one of the few regions where mean circulation is important to the anomaly heat budget.

As mentioned above, previous studies have demonstrated the importance of spatial scale in evaluating the balance between atmosphere- and ocean-driven variability in the ocean heat budget. Bishop et al. (2017) used lagged correlations between surface heat flux and SST, as well as SST tendency, to classify SST variability as being either ocean-driven (e.g., by advection) or atmosphere-driven (i.e., by surface heat flux). Strong positive correlation between SST and surface heat flux at zero lag in the western boundary currents (WBCs) and the ACC demonstrates that SST variability is ocean-driven in these regions. These findings are supported by our results, which show low covariance ratios in forcing and high covariance ratios in advection for these regions. Furthermore, Bishop et al. (2017) showed a clear dependence on spatial scale, such that they see a transition from ocean- to atmosphere-driven regime between 1°and 3°. By focusing on zonal means instead of specific regions such as the WBC extensions and ACC, we did not observe a strong dependence on spatial scale.

Bishop et al. (2017) also show weak correlation at zero lag between SST tendency and surface heat flux in the tropics, which demonstrates that surface heat flux has little effect on the tendency. This is consistent with our observation of covariance ratios for forcing that are close to zero in the tropics. It is likely that their correlations between SST and surface heat flux in the tropics are comparable to the ones in WBCs and ACC when the correlations are normalized to overall variability (Small et al. 2019). The analysis by Bishop et al. (2017) has been extended by Small et al. (2019), who used climate model simulations in addition to observational data. Their analysis employed both relatively low-resolution (1°) and eddy-resolving (0.1°) ocean grids in order to determine the drivers of variability in latent heat flux (LHF). They show that intrinsic ocean variability is much more important in the high-resolution model setup and observational products compared to the standard model resolution of 1°. SST and LHF are positively correlated in equatorial regions and areas with strong temperature gradients, which means that in these regions LHF is ocean-driven.

Similar to our study, Small et al. (2020) evaluated ocean heat budgets over the upper 50 m and 400 m, using both a high- and low-resolution setup. An important insight regarding the impact of resolution arise when performing spatial smoothing with their high-resolution model output to determine at what scale the high-resolution model results reflect the low-resolution results. They found that for most regions this occurs when averaging over a box of 3° to 5° for the 50 m budget and 5° to 7° for the 400 m budget. As most of the sensitivity to spatial resolution lies below 1° (Bishop et al. 2017; Small et al. 2020), it makes sense that the spatial aggregation with ECCOv4 did not lead to large differences globally, as the spatial resolution of ECCOv4 is around 1°.

This suggests that higher spatial resolution is necessary to capture intrinsically ocean-driven heat content variability. However, it is currently not feasible in a reanalysis framework to present estimates at resolution below 1° and ensure constraining them to available observations. Despite these limitations, ECCOv4 presents a distinct advantage in that it is a physically consistent estimate of the observed ocean state. It accurately reflects the ocean variability over larger region, though it must be recognized that once the spatial resolution is increased, intrinsic ocean variability will likely play a more important role in characterizing overall variability.

The work we presented here includes novel approaches that complement previous work describing factors influencing the ocean heat budget. By employing ECCOv4, which is constrained by observations in a physically consistent way, our work closely reflects the real ocean state, in that the variability of our model resembles the observational record, such as from Argo floats. Furthermore, the temporal decomposition of the mean versus anomalous heat advection provided new insights in the ocean heat variability. In particular, the decomposition allowed us to see that most of the ocean heat variability is due to anomalies in the circulation, while anomalies in the temperature field have an effect in focused regions and become more relevant on interannual timescales.

Data availability statement. All results of this study are based on ECCO Version 4, Release 3 (ECCOv4r3) for which standard output and documentation can be obtained at `https://ecco.jpl.nasa.gov/drive/files/Version4/Release3/`. We reproduced the ECCOv4r3 ocean state estimate with a custom set of diagnostics which are available as a dataset on Pangeo (`http://catalog.pangeo.io/ocean/ECCOv4r3`) or can be requested from the corresponding author.

Acknowledgments. JET acknowledges funding from NASA's Goddard Space Flight Center (Award NNX15AN27H). RPA acknowledges support from NSF Award OCE-1553593 and a Sloan Fellowship in Ocean Sciences. Computational tools for performing this research were provided by Pangeo, supported by NSF EarthCube award OCE-1740648. The authors thank Spencer Jones for providing helpful comments.

References

Adcroft, A., and J.-M. Campin, 2004: Rescaled height coordinates for accurate representation of free-surface flows in ocean circulation models. *Ocean Modelling*, **7 (3)**, 269–284, doi:10.1016/j.ocemod.2003.09.003.

Alexander, M. A., and C. Deser, 1995: A Mechanism for the Recurrence of Wintertime Midlatitude SST Anomalies. *Journal of Physical Oceanography*, **25 (1)**, 122–137, doi:

10.1175/1520-0485(1995)025<0122:AMFTRO>2.0.CO;2.

Armour, K. C., J. Marshall, J. R. Scott, A. Donohoe, and E. R. Newsom, 2016: Southern Ocean warming delayed by circumpolar upwelling and equatorward transport. *Nature Geoscience*, **9 (7)**, 549–554.

Barnett, T. P., D. W. Pierce, K. M. AchutaRao, P. J. Gleckler, B. D. Santer, J. M. Gregory, and W. M. Washington, 2005: Penetration of Human-Induced Warming into the World's Oceans. *Science*, **309 (5732)**, 284–287, doi:10.1126/science.1112418.

Barnett, T. P., D. W. Pierce, and R. Schnur, 2001: Detection of Anthropogenic Climate Change in the World's Oceans. *Science*, **292 (5515)**, 270–274, doi:10.1126/science.1058304.

Bigg, G. R., T. D. Jickells, P. S. Liss, and T. J. Osborn, 2003: The role of the oceans in climate. *International Journal of Climatology*, **23 (10)**, 1127–1159, doi:10.1002/joc.926.

Bishop, S. P., R. J. Small, F. O. Bryan, and R. A. Tomas, 2017: Scale Dependence of Midlatitude Air–Sea Interaction. *Journal of Climate*, **30 (20)**, 8207–8221.

Buckley, M. W., R. M. Ponte, G. Forget, and P. Heimbach, 2014: Low-Frequency SST and Upper-Ocean Heat Content Variability in the North Atlantic. *Journal of Climate*, **27 (13)**, 4996–5018, doi:10.1175/JCLI-D-13-00316.1.

Buckley, M. W., R. M. Ponte, G. Forget, and P. Heimbach, 2015: Determining the Origins of Advective Heat Transport Convergence Variability in the North Atlantic. *Journal of Climate*, **28 (10)**, 3943–3956, doi:10.1175/JCLI-D-14-00579.1.

Campin, J.-M., A. Adcroft, C. Hill, and J. Marshall, 2004: Conservation of properties in a free-surface model. *Ocean Modelling*, **6 (3)**, 221–244, doi:10.1016/S1463-5003(03)00009-X.

Carmack, E. C., and Coauthors, 2015: Toward Quantifying the Increasing Role of Oceanic Heat in Sea Ice Loss in the New Arctic. *Bulletin of the American Meteorological Society*, **96 (12)**, 2079–2105, doi:10.1175/BAMS-D-13-00177.1.

Cayan, D. R., 1992: Latent and Sensible Heat Flux Anomalies over the Northern Oceans: Driving the Sea Surface Temperature. *Journal of Physical Oceanography*, **22 (8)**, 859–881, doi:10.1175/1520-0485(1992)022<0859:LASHFA>2.0.CO;2.

Church, J. A., and Coauthors, 2013: Sea level change. *Climate Change 2013: The physical science basis. Contribution of Working Group I to the Fifth Assessment Report of the Intergovernmental Panel on Climate Change*, T. Stocker, D. Qin, G.-K. Plattner, M. Tignor, S. Allen, J. Boschung, A. Nauels, Y. Xia, V. Bex, and P. Midgley, Eds., Cambridge University Press, Cambridge, United Kingdom and New York, NY, USA, 1137–1216.

Doney, S. C., S. Yeager, G. Danabasoglu, W. G. Large, and J. C. McWilliams, 2007: Mechanisms Governing Interannual Variability of Upper-Ocean Temperature in a Global Ocean Hindcast Simulation. *Journal of Physical Oceanography*, **37 (7)**, 1918–1938.

Forget, G., J.-M. Campin, P. Heimbach, C. N. Hill, R. M. Ponte, and C. Wunsch, 2015: ECCO version 4: an integrated framework for non-linear inverse modeling and global ocean state estimation. *Geoscientific Model Development*, **8 (10)**, 3071–3104, doi:10.5194/gmd-8-3071-2015.

Gill, A. E., and P. P. Niller, 1973: The theory of the seasonal variability in the ocean. *Deep-Sea Research and Oceanographic Abstracts*, **20 (2)**, 141–177, doi:10.1016/0011-7471(73)90049-1.

Gregory, J. M., H. T. Banks, P. A. Stott, J. A. Lowe, and M. D. Palmer, 2004: Simulated and observed decadal variability in ocean heat content. *Geophysical Research Letters*, **31 (15)**, doi:10.1029/2004GL020258.

Grist, J. P., and Coauthors, 2010: The roles of surface heat flux and ocean heat transport convergence in determining Atlantic Ocean temperature variability. *Ocean Dynamics*, **60 (4)**, 771–790.

Hasselmann, K., 1976: Stochastic climate models, Part I. Theory. *Tellus*, **28 (6)**, 473–485, doi: 10.1111/j.2153-3490.1976.tb00696.x.

Holland, D. M., R. H. Thomas, B. de Young, M. H. Ribergaard, and B. Lyberth, 2008: Acceleration of Jakobshavn Isbræ triggered by warm subsurface ocean waters. *Nature Geoscience*, **1 (10)**, 659–664, doi:10.1038/ngeo316.

Jackson, L. C., K. A. Peterson, C. D. Roberts, and R. A. Wood, 2016: Recent slowing of Atlantic overturning circulation as a recovery from earlier strengthening. *Nature Geoscience*, **9 (7)**, 518–522, doi:10.1038/ngeo2715.

Keenlyside, N. S., M. Latif, J. Jungclaus, L. Kornblueh, and E. Roeckner, 2008: Advancing decadal-scale climate prediction in the North Atlantic sector. *Nature*, **453**, 84–88, doi:10.1038/nature06921.

Kirtman, B. P., and Coauthors, 2012: Impact of ocean model resolution on CCSM climate simulations. *Climate Dynamics*, **39 (6)**, 1303–1328, doi:10.1007/s00382-012-1500-3.

Levitus, S., J. Antonov, and T. Boyer, 2005: Warming of the world ocean, 1955âĂŞ2003. *Geophysical Research Letters*, **32 (2)**, doi:10.1029/2004GL021592.

Levitus, S., and Coauthors, 2012: World ocean heat content and thermosteric sea level change (0-2000 m), 1955-2010. *Geophysical Research Letters*, **39 (10)**, doi:10.1029/2012GL051106.

Liang, X., C. Wunsch, P. Heimbach, and G. Forget, 2015: Vertical Redistribution of Oceanic Heat Content. *Journal of Climate*, **28 (9)**, 3821–3833, doi:10.1175/JCLI-D-14-00550.1.

Liu, W., and S.-P. Xie, 2018: An Ocean View of the Global Surface Warming Hiatus. *Oceanography*, **31 (2)**, 72–79, doi:10.5670/oceanog.2018.217.

Menary, M. B., L. Hermanson, and N. J. Dunstone, 2016: The impact of Labrador Sea temperature and salinity variability on density and the subpolar AMOC in a decadal prediction system. *Geophysical Research Letters*, **43 (23)**, 12 217–12 227, doi:10.1002/2016GL070906.

Piecuch, C. G., and R. M. Ponte, 2012: Importance of Circulation Changes to Atlantic Heat Storage Rates on Seasonal and Interannual Time Scales. *Journal of Climate*, **25 (1)**, 350–362, doi:10.1175/JCLI-D-11-00123.1.

Piecuch, C. G., R. M. Ponte, C. M. Little, M. W. Buckley, and I. Fukumori, 2017: Mechanisms underlying recent decadal changes in subpolar North Atlantic Ocean heat content. *Journal of Geophysical Research: Oceans*, **122 (9)**, 7181–7197, doi:10.1002/2017JC012845.

Pierce, D. W., T. P. Barnett, K. M. AchutaRao, P. J. Gleckler, J. M. Gregory, and W. M. Washington, 2006: Anthropogenic Warming of the Oceans: Observations and Model Results. *Journal of Climate*, **19 (10)**, 1873–1900, doi:10.1175/JCLI3723.1.

Pierce, D. W., P. J. Gleckler, T. P. Barnett, B. D. Santer, and P. J. Durack, 2012: The fingerprint of human-induced changes in the ocean's salinity and temperature fields. *Geophysical Research Letters*, **39 (21)**, doi:10.1029/2012GL053389.

Roberts, C. D., D. Calvert, N. Dunstone, L. Hermanson, M. D. Palmer, and D. Smith, 2016: On the Drivers and Predictability of Seasonal-to-Interannual Variations in Regional Sea Level. *Journal of Climate*, **29 (21)**, 7565–7585, doi:10.1175/JCLI-D-15-0886.1.

Roberts, C. D., M. D. Palmer, R. P. Allan, D. G. Desbruyeres, P. Hyder, C. Liu, and D. Smith, 2017: Surface flux and ocean heat transport convergence contributions to seasonal and interannual variations of ocean heat content. *Journal of Geophysical Research: Oceans*, **122 (1)**, 726–744, doi:10.1002/2016JC012278.

Robson, J., P. Ortega, and R. Sutton, 2016: A reversal of climatic trends in the North Atlantic since 2005. *Nature Geoscience*, **9**, 513–517, doi:10.1038/ngeo2727.

Robson, J. I., R. T. Sutton, and D. M. Smith, 2012: Initialized decadal predictions of the rapid warming of the North Atlantic Ocean in the mid 1990s. *Geophysical Research Letters*, **39 (19)**, doi:10.1029/2012GL053370.

Small, R. J., F. O. Bryan, S. P. Bishop, S. Larson, and R. A. Tomas, 2020: What drives upper ocean temperature variability in coupled climate models and observations? *Journal of Climate*, **33 (2)**, 577–596, doi:10.1175/JCLI-D-19-0295.1.

Small, R. J., R. A. Tomas, F. O. Bryan, and S. P. Bishop, 2019: Air-sea turbulent heat fluxes in climate models and observational analyses: what drives their variability? *Journal of Climate*, **32 (8)**, 2397–2421, doi:10.1175/JCLI-D-18-0576.1.

Straneo, F., and P. Heimbach, 2013: North Atlantic warming and the retreat of Greenland's outlet glaciers. *Nature*, **504 (7478)**, 36–43, doi:10.1038/nature12854.

Trenberth, K. E., J. T. Fasullo, and M. A. Balmaseda, 2014: Earth's Energy Imbalance. *Journal of Climate*, **27 (9)**, 3129–3144, doi:10.1175/JCLI-D-13-00294.1.

von Schuckmann, K., and Coauthors, 2016: An imperative to monitor Earth's energy imbalance. *Nature Climate Change*, **6**, 138–144, doi:10.1038/nclimate2876.

von Storch, J.-S., 2000: Signatures of Air-Sea Interactions in a Coupled Atmosphere-Ocean GCM. *Journal of Climate*, **13 (1)**, 3361–3379, doi:10.1175/1520-0442(2000)013<3361:SOASII>2.0.CO;2.

Warren, B. A., 1999: Approximating the energy transport across oceanic sections. *Journal of Geophysical Research: Oceans*, **104 (C)**, 7915–7919, doi:10.1029/1998JC900089.

Wu, R., B. P. Kirtman, and K. Pegion, 2006: Local Air-Sea Relationship in Observations and Model Simulations. *Journal of Climate*, **19 (19)**, 4914–4932, doi:10.1175/JCLI3904.1.

Yan, X.-H., T. Boyer, K. Trenberth, T. R. Karl, S.-P. Xie, V. Nieves, K.-K. Tung, and D. Roemmich, 2016: The global warming hiatus: Slowdown or redistribution? *Earth's Future*, **4 (11)**, 472–482, doi:10.1002/2016EF000417.

Zanna, L., S. Khatiwala, J. M. Gregory, J. Ison, and P. Heimbach, 2019: Global reconstruction of historical ocean heat storage and transport. *Proceedings of the National Academy of Sciences*, **116 (4)**, 1126–1131, doi:10.1073/pnas.1808838115.

LIST OF TABLES

Table 1. Ocean regions considered in the study and corresponding abbreviations.

Name	**Abbreviation**
Pacific Ocean	pac
North Pacific Ocean	npac
Tropical Pacific Ocean	tropac
South Pacific Ocean	spac
Atlantic Ocean	atl
North Atlantic Ocean	natl
Tropical Atlantic Ocean	troatl
South Atlantic Ocean	satl
Indian Ocean	ind
Tropical Indian Ocean	troind
South Indian Ocean	sind
Southern Ocean	so
Subpolar North Atlantic	spna

TABLE 2. Covariance ratios for heat budget terms for different ocean basins, subsections and specific ocean regions. Monthly heat budget terms were integrated over the upper 700 m. The first four rows present covariance ratios for the major terms, and the remaining rows present covariance ratios for different advection terms as described in Equation 2. Columns represent ocean basins and sections as defined in Figure 1 and Table 1.

	pac	**npac**	**tropac**	**spac**	**atl**	**natl**	**troatl**	**satl**	**ind**	**troind**	**sind**	**so**	**spna**
Forcing	0.805	0.373	0.426	0.470	0.848	0.852	0.461	0.732	0.699	0.361	0.684	0.671	0.740
Advection	0.194	0.627	0.572	0.529	0.155	0.154	0.538	0.266	0.299	0.636	0.315	0.333	0.286
Diffusion	0.000	−0.000	−0.000	0.001	−0.003	−0.006	0.001	0.001	0.001	0.002	0.000	−0.006	−0.025
Residual	0.001	0.000	0.002	0.001	−0.000	0.001	0.000	0.001	0.001	0.001	0.001	0.002	−0.001
$\nabla(\mathbf{u}'\overline{\theta}^m)$	0.190	0.628	0.584	0.522	0.138	0.161	0.556	0.240	0.277	0.674	0.277	0.299	0.277
$\nabla(\overline{\mathbf{u}}^m\theta')$	0.005	−0.003	−0.012	0.008	0.019	−0.011	−0.020	0.026	0.018	−0.043	0.035	0.029	0.006
$\nabla(\mathbf{u}'\theta' - \overline{\mathbf{u}'\theta'}^m)$	−0.000	0.002	0.000	-0.001	-0.001	0.004	0.001	-0.001	0.004	0.005	0.003	0.004	0.002
$\nabla_h(\mathbf{u}'\overline{\theta}^m)$	0.234	0.807	0.768	0.696	0.077	0.240	0.738	0.323	0.339	0.923	0.461	0.383	0.456
$\frac{\partial}{\partial z}(w'\overline{\theta}^m)$	−0.044	−0.179	−0.184	−0.175	0.060	−0.079	−0.183	-0.083	−0.062	−0.248	−0.184	−0.084	−0.178
$\nabla_h(\overline{\mathbf{u}}^m\theta')$	0.003	−0.004	−0.013	0.009	0.018	−0.013	−0.019	0.027	0.019	−0.042	0.034	0.030	0.001
$\frac{\partial}{\partial z}(\overline{w}^m\theta')$	0.002	0.000	0.001	−0.001	0.001	0.002	−0.000	−0.000	−0.001	−0.001	0.001	−0.001	0.005

TABLE 3. Global average covariance ratios for heat budget terms at different spatial aggregation. Monthly heat budget terms were integrated over the upper 700 m. The aggregation value refers to the level of binning, where $n \times n$ aggregation indicates grouping of n grid cells along both x and y in the horizontal space.

Aggregation	F'_{forc}	$-\nabla\cdot\mathbf{F}_{\text{diff}}'$	$-\nabla_h\cdot(\mathbf{u}'\overline{\theta}^m)$	$-\frac{\partial}{\partial z}(w'\overline{\theta}^m)$	$-\nabla_h\cdot(\overline{\mathbf{u}}^m\theta')$	$-\frac{\partial}{\partial z}(\overline{w}^m\theta')$	$-\nabla\cdot(\mathbf{u}'\theta'-\overline{\mathbf{u}'\theta'}^m)$	Residual
1×1	0.234	0.003	0.906	−0.229	0.072	0.000	0.007	0.006
2×2	0.237	0.003	0.909	−0.230	0.069	0.000	0.007	0.005
3×3	0.245	0.002	0.906	−0.230	0.067	0.000	0.007	0.004
5×5	0.263	0.001	0.897	−0.229	0.059	0.000	0.006	0.003
6×6	0.272	0.001	0.889	−0.227	0.056	0.000	0.005	0.003
9×9	0.301	−0.000	0.870	−0.224	0.046	0.000	0.005	0.002
10×10	0.309	0.000	0.860	−0.220	0.044	0.000	0.005	0.002
15×15	0.341	−0.001	0.827	−0.214	0.040	0.000	0.004	0.002
18×18	0.354	−0.000	0.812	−0.206	0.034	0.000	0.005	0.002
30×30	0.383	−0.000	0.777	−0.199	0.033	0.000	0.003	0.002
45×45	0.427	−0.001	0.714	−0.176	0.030	0.000	0.005	0.002

LIST OF FIGURES

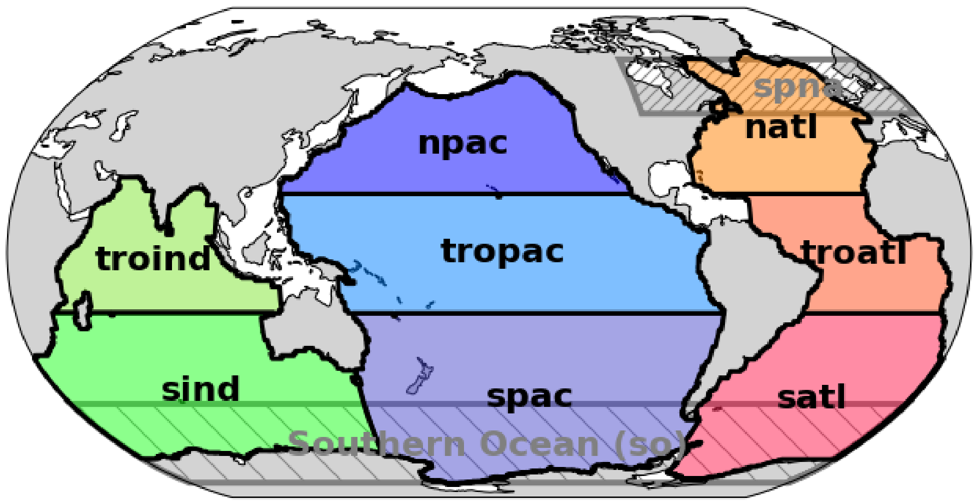

FIG. 1. Definition of ocean regions for which basin-scale heat budgets are analyzed. The regions are North Pacific (npac), Tropical Pacific (tropac), South Pacific (spac), Tropical Indian Ocean (troind), South Indian ocean (sind), North Atlantic (natl), Tropical Atlantic (troatl) and South Atlantic (satl). The spatial domain of the subpolar North Atlantic (spna) and Southern Ocean (so) are indicated as grey boxes.

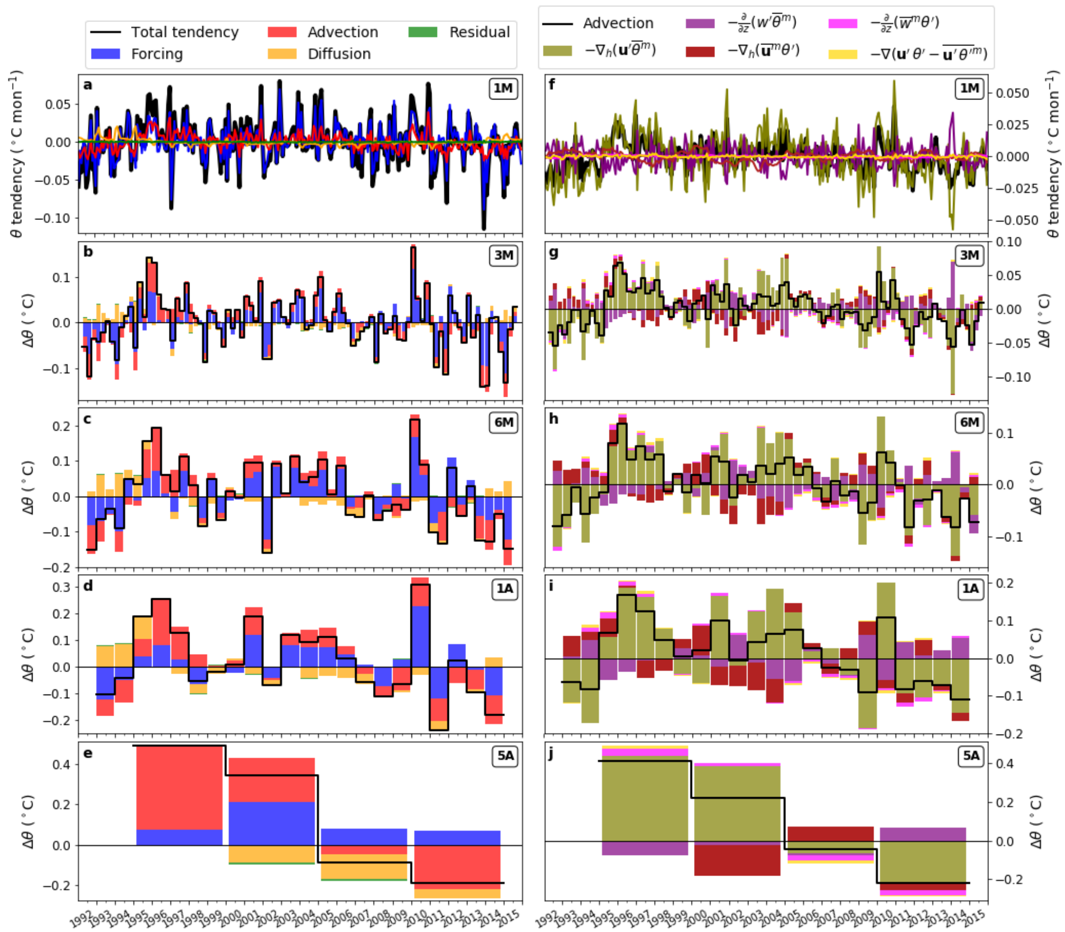

842 FIG. 2. Time series for the temperature budget of the subpolar North Atlantic (spna) shown for different temporal aggregation scales. The top panels (a, f) show the monthly resolution while lower panels show aggregation scales of (b, g) 3-month (3M), (c, h) 6-month (6M), (d, i) annual (1A) and (e, j) pentad (5A) aggregations. The panels on the left (a-e) show the balance between the total tendency of temperature and the three major terms in the budget equation. In all cases, the total tendency (black) is balanced by the individual contributions by forcing (blue), advection (red), and diffusion (orange). A residual term is included (green) to indicate any unaccounted contributions (e.g., due to neglecting submonthly covariation between temperature and velocity). The panels on the right (f-j) show the decomposition of the advection into the different terms as described in Equation 2, where total advection (black) is equal to the sum of the horizontal and vertical components of the anomalous circulation of mean temperature (olive-green and purple), the horizontal and vertical components of the mean circulation of anomalous temperature (dark red and magenta), and a nonlinear term arising from the possible correlation between anomalous circulation and anomalous temperature (yellow). Note that the units describe temperature change over the given time interval, where for monthly resolution (a, f) the tendencies are given as °C per month and the other cases are given as °C over the given aggregation time interval.

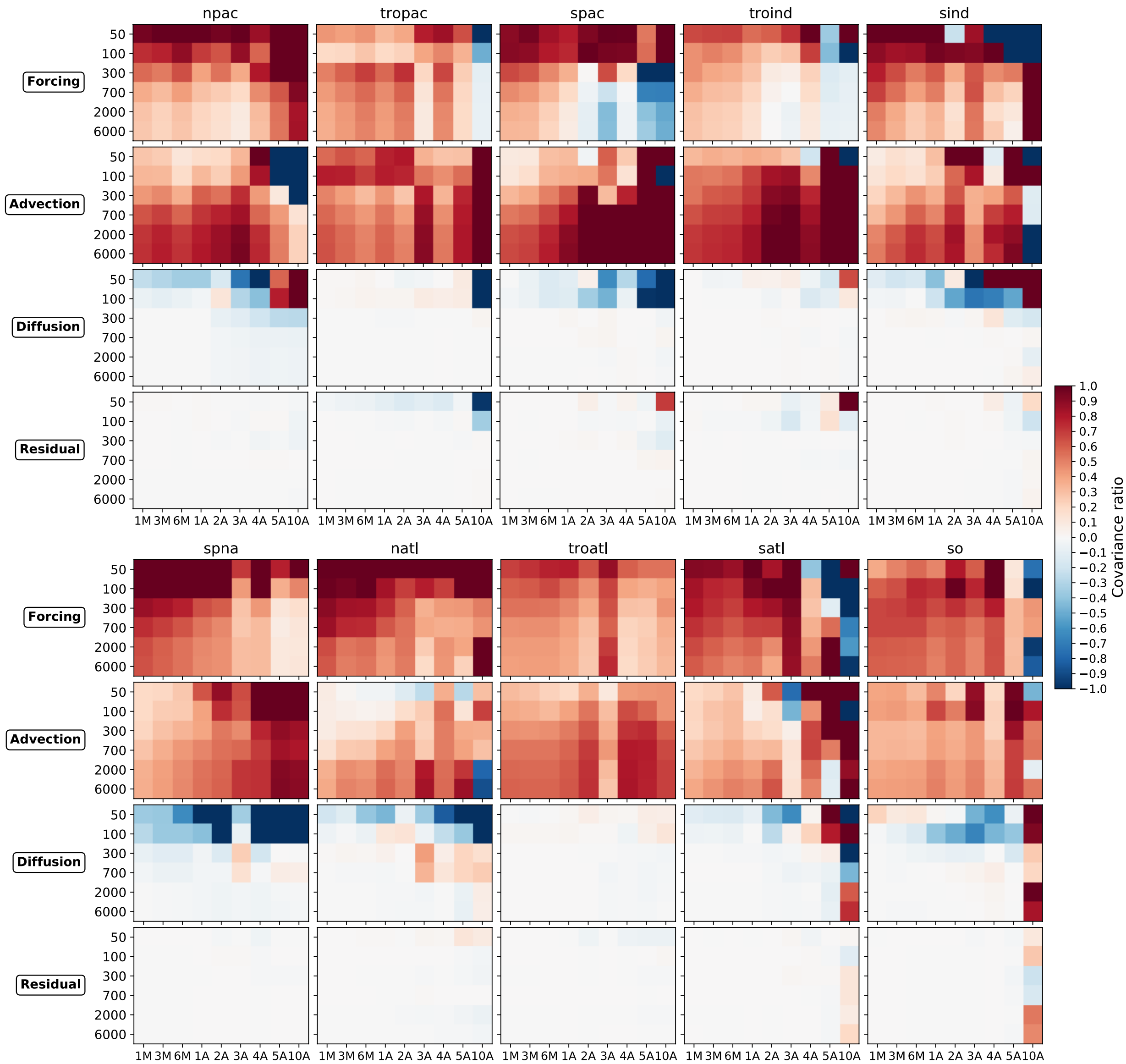

856 FIG. 3. Covariance ratio for the different ocean regions at different integration depths (50 m, 100 m, 300 m, 700 m, 2000 m and 6000 m) and time aggregation scales (1M, 3M, 6M, 1A, 2A, 3A, 4A, 5A, 10A). Each column of four panels represents the four heat budget terms (forcing, advection, diffusion, residual) for an ocean region. Each panel sorts the covariance ratio for each term by integration depth along the vertical axis and time aggregation scale along the horizontal axis.

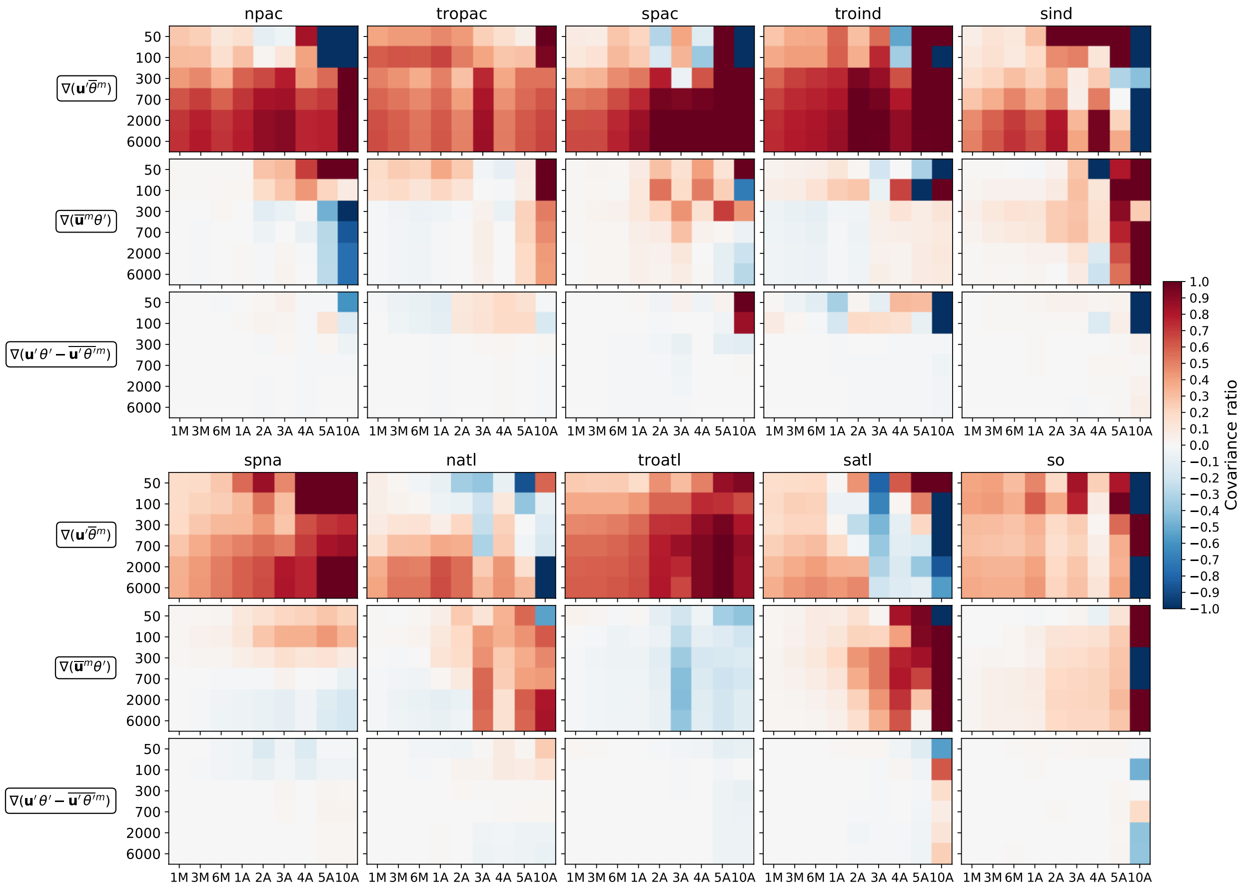

FIG. 4. Covariance ratio for the different ocean regions at different integration depths (50 m, 100 m, 300 m, 700 m, 2000 m and 6000 m) and time aggregation scale (1M, 3M, 6M, 1A, 2A, 3A, 4A, 5A, 10A). Each column of three panels represents the decomposed terms for advection for an ocean region. Each panel sorts the covariance ratio for each term by integration depth along the vertical axis and time aggregation scale along the horizontal axis.

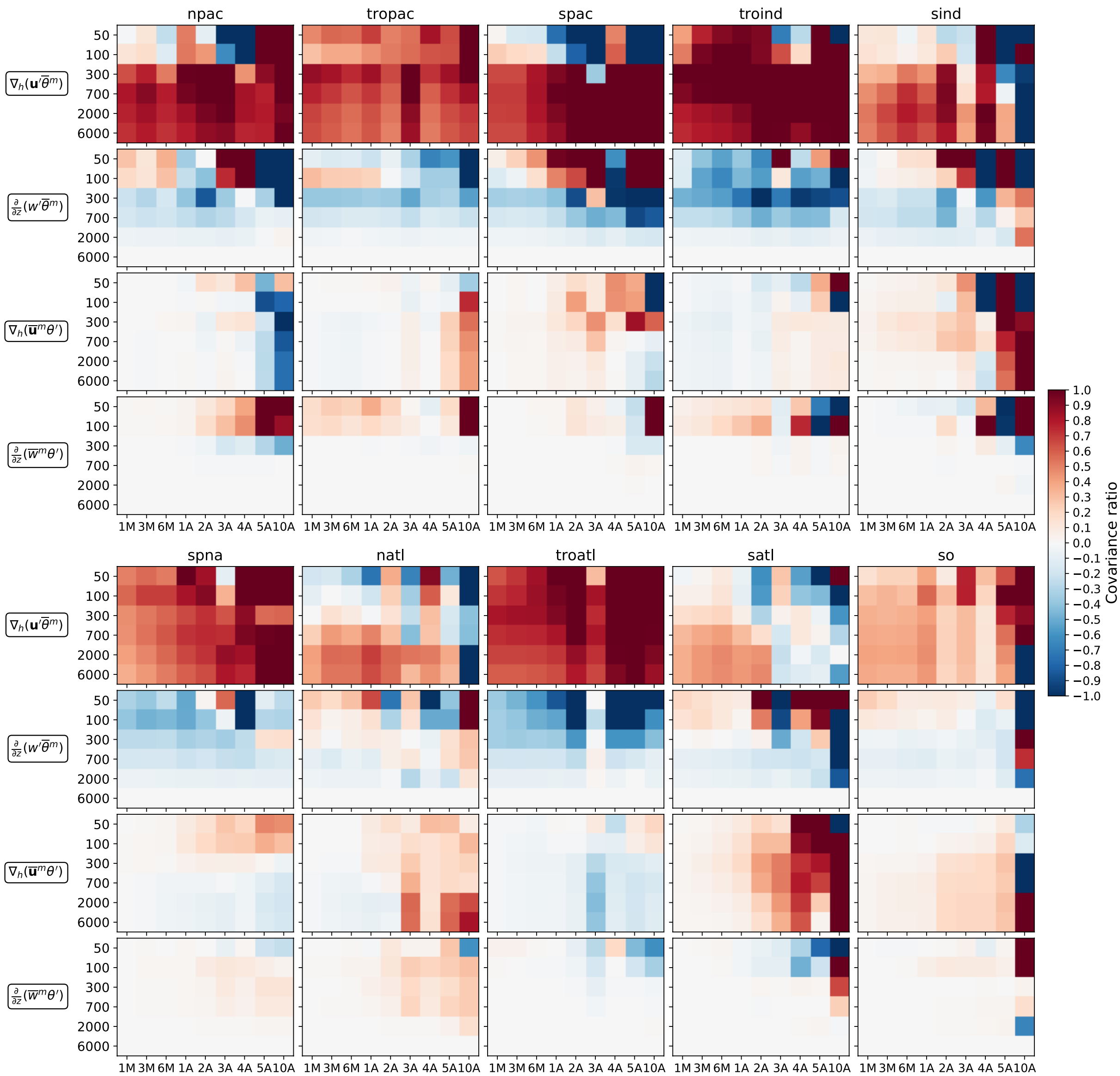

FIG. 5. Covariance ratio for the different ocean regions at different integration depths (50 m, 100 m, 300 m, 700 m, 2000 m and 6000 m) and time aggregation scale (1M, 3M, 6M, 1A, 2A, 3A, 4A, 5A, 10A). Each column of four panels represents the horizontal and vertical component of the linear terms for advection for an ocean region. Each panel sorts the covariance ratio for each term by integration depth along the vertical axis and time aggregation scale along the horizontal axis.

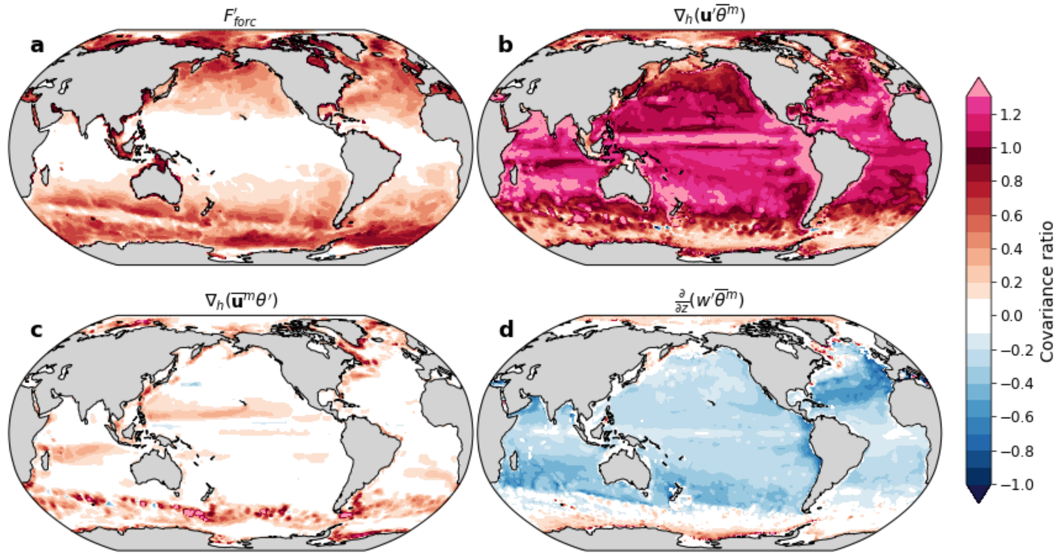

FIG. 6. Global distribution of the covariance ratio between the total tendency and (a) forcing, (b) anomalous horizontal advection of mean temperature field, (c) mean horizontal advection of anomalous temperature field and (d) anomalous vertical advection of mean temperature field. The terms are integrated over the upper 700 m of ocean and the covariance ratios have been evaluated on the original spatial and temporal resolution.

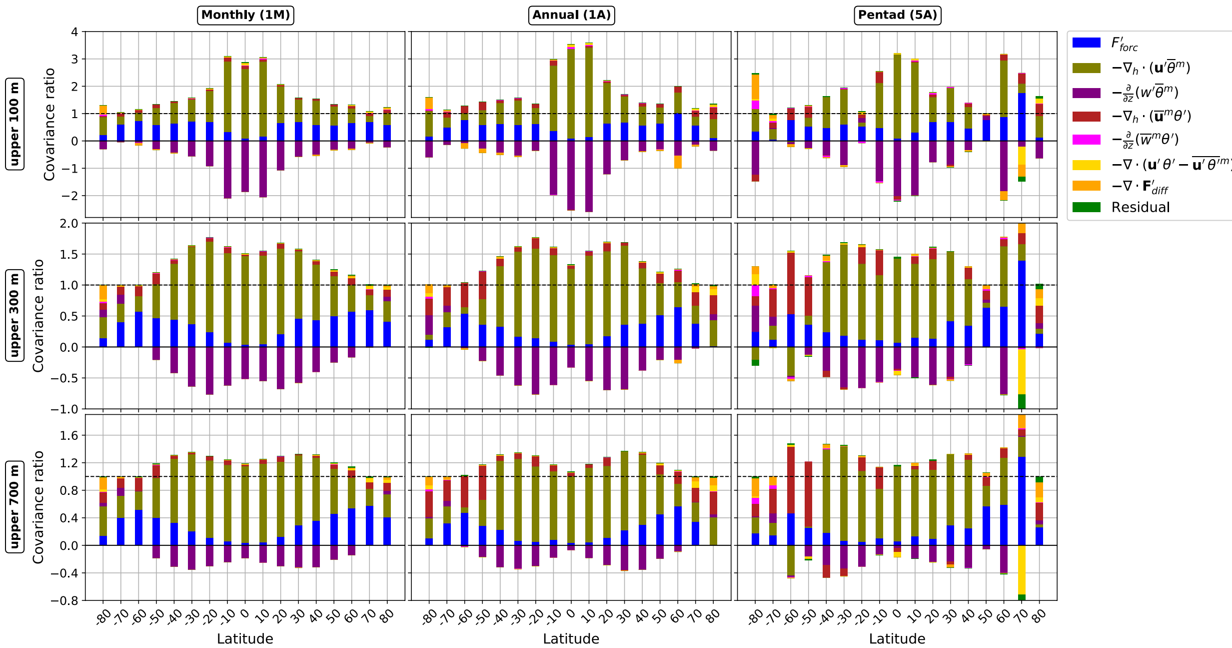

FIG. 7. Zonal means of the covariance ratios for the different budget terms in the upper 100 m (top row), 300 m (center row) and 700 m (bottom row), and for monthly (left column), annual (middle column) and pentad (right column) temporal averages. Covariance ratios were derived from the original (1 × 1) spatial resolution and averaged into 10° latitude bins.

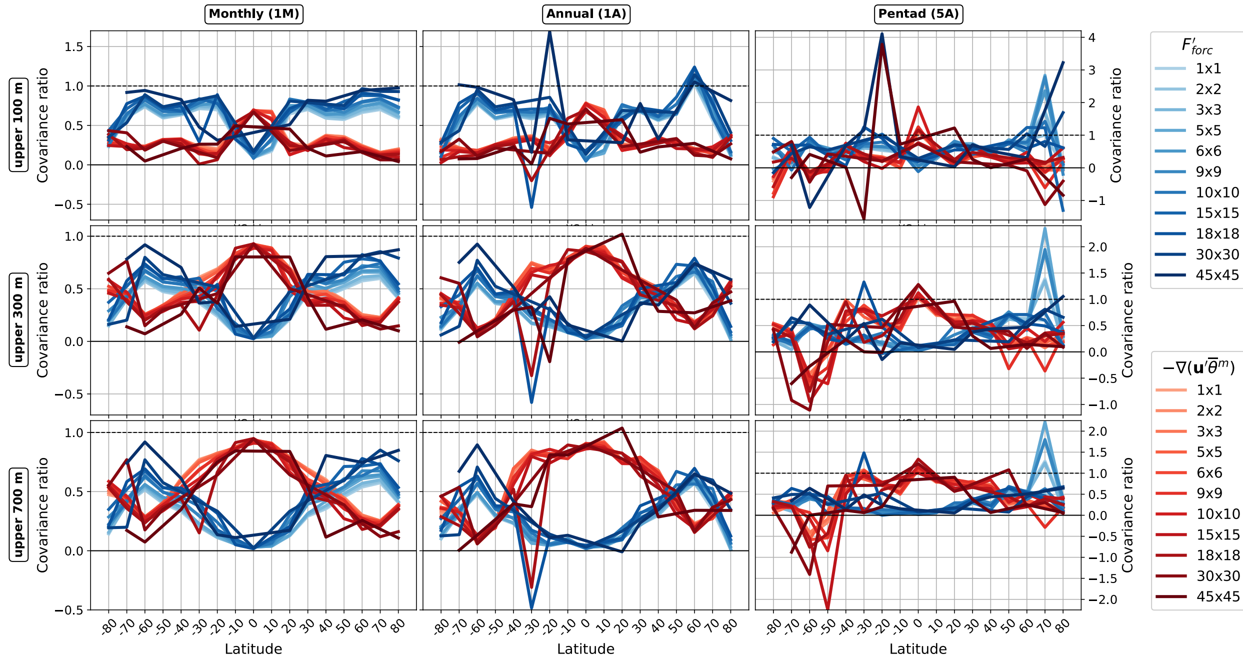

879 FIG. 8. Zonal means of the covariance ratios for forcing ($F_{\mathrm{forc}}{}'$, blue lines) and anomalous advection $-\nabla\cdot(\mathbf{u}'\overline{\theta}^m)$ (red lines). Lines are shaded by spatial aggregation scale with darker shades corresponding to coarser aggregations. Covariance ratios were derived from $F_{\mathrm{forc}}{}'$ and $-\nabla\cdot(\mathbf{u}'\overline{\theta}^m)$ at each aggregation scale and averaged into 10° latitude bins. Zonal means are presented for the upper 100 m (top row), 300 m (center row) and 700 m (bottom row), as well as using monthly (left column), annual (middle column) and pentad (right column) temporal averages.